

Magnetic and physical properties of new hexagonal compounds PrPt_4X ($X = \text{Ag}, \text{Au}$)

Michael O Ogunbunmi and André M Strydom

Highly Correlated Matter Research Group, Physics Department, University of Johannesburg,
P. O. Box 524, Auckland Park 2006, South Africa.

E-mail: mogunbunmi@uj.ac.za, moogunbunmi@gmail.com

Abstract. We have synthesized PrPt_4Ag and PrPt_4Au compounds for the first time and report their crystal structure, as well as magnetic and physical properties in the temperature range of 1.9 K to 300 K. Both compounds are derived from the substitution of Pt with Ag and Au, respectively in the parent compound PrPt_5 which crystallizes in the hexagonal CaCu_5 -type structure. Here we observed the preservation of the hexagonal CaCu_5 -type structure under such substitutions, which is in contrast to the observations in PrCu_4Ag and PrCu_4Au adopting the cubic MgCu_4Sn -type structure upon substitution on parent hexagonal PrCu_5 . The temperature dependences of specific heat $C_p(T)$, and electrical resistivity $\rho(T)$ of PrPt_4Ag show an anomaly at 7.6 K. This is absent in the magnetic susceptibility $\chi(T)$, thus suggesting a possible multipolar ordering of the Pr^{3+} moment. PrPt_4Au on the other hand does not show any anomaly but an upturn in $C_p(T)/T$ below about 10 K and attains $1.23 \text{ J}/(\text{mol K}^2)$ at 1.9 K. In addition, $\rho(T) \sim T$ for nearly a decade in temperature. These observations for PrPt_4Au are the hallmark of a non-Fermi liquid (nFL) behavior and is characteristic of a system near a quantum critical point. The analyses of the low-temperature $C_p(T)$ for PrPt_4Ag and PrPt_4Au give values of the Sommerfeld coefficient, $\gamma = 728.5 \text{ mJ}/(\text{mol K}^2)$ and $509.1 \text{ mJ}/(\text{mol K}^2)$, respectively, indicating a significant enhancement of the quasiparticle mass in the two compounds.

1. Introduction

PrPt_5 is a Van-Vleck paramagnet that has been studied mostly for nuclear cooling by adiabatic demagnetization [1]. This technique profits from the high nuclear spin ($I = 5/2$) of the only known stable ^{141}Pr isotope. It crystallizes in the hexagonal CaCu_5 -type structure with space group $P6/mmm$ (No. 191) [2]. It has been observed that the lack of magnetic ordering in PrPt_5 is associated with its weak exchange interaction [3]. In addition, magnetization studies have revealed a nuclear spontaneous ferromagnetic Weiss temperature, $\theta_p = 2 \text{ mK}$, which is attributed to nuclear hyperfine enhancement in the system [4]. In a substitution study by Malik *et al.* [5], the $R\text{Pt}_4\text{In}$ ($R = \text{La-Tm}$) compounds, which represent a doping of 20% on the Pt site, were reported to adopt the cubic MgCu_4Sn -type structure with the exception of TmPt_4In which forms in the Cu_3Au -type structure. Also, ErPt_4In and HoPt_4In were observed to possess a mixture of MgCu_4Sn and Cu_3Au phases as evidenced from the X-ray diffraction patterns. PrPt_4In was reported to remain paramagnetic down to 4.2 K [5]. Here we report the synthesis, as well as the magnetic and physical properties of the new compounds PrPt_4Ag and PrPt_4Au . Interestingly, it was found that both compounds crystallize in the same hexagonal CaCu_5 parent structure. This is in contrast with the observations in PrCu_4Ag and PrCu_4Au [6, 7] which adopt

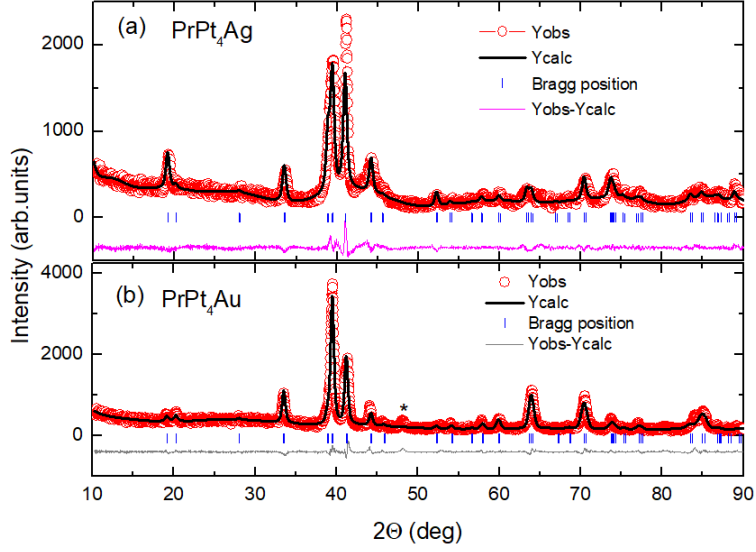


Figure 1. Powder X-ray diffraction patterns of PrPt_4Ag and PrPt_4Au shown in (a) and (b) with Rietveld refinements (black lines) based on the $P6/mmm$ space group. The vertical bars are the Bragg peak positions, while the difference between the experimental and calculated intensities are shown as pink and gray lines, respectively. The peak in the PrPt_4Au spectrum marked with an asterisk does not belong to the major phase as discussed in the text.

the cubic MgCu_4Sn -type structure similar to those of $R\text{Pt}_4\text{In}$ compounds reported by Malik *et al.* [5].

2. Experimental methods

Polycrystalline samples of PrPt_4Ag and PrPt_4Au were prepared by arc melting stoichiometric amounts of high-purity elements (wt.% ≥ 99.9) on a water-cooled Cu plate under a purified static argon atmosphere in an Edmund Buehler arc furnace. The weight losses for both compounds were $\sim 0.09\%$. The arc-melted pellets were then wrapped in Ta foil, placed in an evacuated quartz tube and annealed at 800°C for 14 days so as to improve the quality of the samples. Room temperature powder X-ray diffraction (XRD) patterns were recorded on pulverized samples using a Rigaku diffractometer employing $\text{Cu-K}\alpha$ radiation. The XRD patterns with the Rietveld refinements [8] employing the FullProf suite of programs [9] are shown in Fig. 1. The lattice parameters obtained from the Rietveld refinements are presented in Table 1. For both compounds, the XRD results confirm phase formation of the desired compounds. For the case of PrPt_4Au , a spurious peak, barely resolved above the background noise was detected at $2\theta = 48^\circ$. It was verified that this peak does not have its origin in any of the elements Pr, Pt or Au thus the origin of this peak remains unknown.

Magnetic properties were measured using the Magnetic Property Measurement System (Quantum Design Inc., San Diego) between 1.8 K and 300 K with an external magnetic field up to 7 T. The four-probe DC electrical resistivity, specific heat and thermal transport between 1.9 K and 300 K were measured using the Physical Property Measurement System also from Quantum Design.

3. Magnetic properties

The temperature dependences of magnetic susceptibility $\chi(T)$ of both compounds in an external field of 0.1 T are shown in Fig. 2 (a) and (b). From the plots, $\chi(T)$ of both compounds are

Table 1. Lattice parameters of PrPt₄Ag and PrPt₄Au obtained from the Rietveld refinements of their XRD patterns.

Compound	a (Å)	c (Å)	V (Å ³)	R_p (%)	R_{wp} (%)	χ^2
PrPt ₄ Ag	5.344(2)	4.399(2)	108.8(9)	9.597	12.25	4.596
PrPt ₄ Au	5.343(3)	4.378(5)	108.3(8)	8.957	11.89	4.875

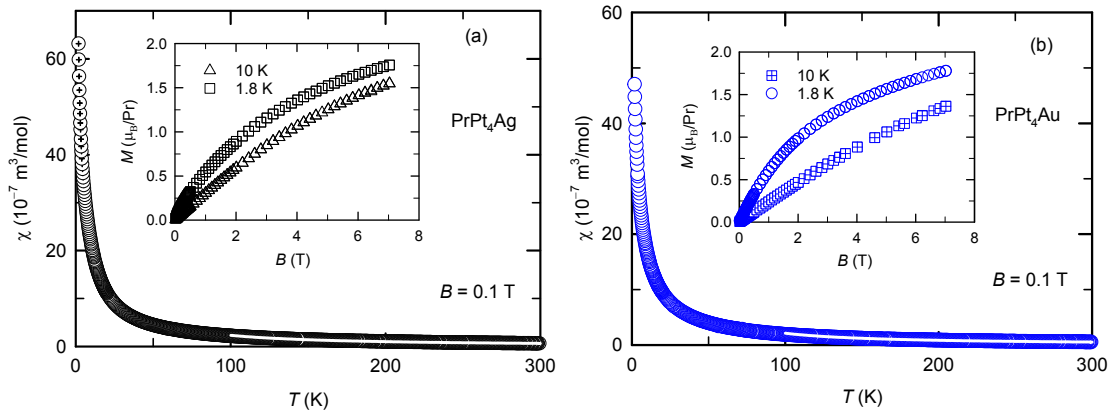


Figure 2. (a) Temperature dependence of magnetic susceptibility $\chi(T)$ of PrPt₄Ag in an external field of 0.1 T with a Curie-Weiss fit shown as a white line. Inset: Isothermal magnetization of PrPt₄Ag at 1.8 K and 10 K. (b) Plot of χ against T for PrPt₄Au with a Curie-Weiss fit represented by the white line. Inset: Isothermal magnetization of PrPt₄Au at 1.8 K and 10 K.

qualitatively similar and show no visible anomaly down to 1.9 K. For temperatures above 100 K, $\chi(T)$ for both compounds follow a Curie-Weiss behavior based on the expression: $\chi(T) = N_A \mu_{\text{eff}}^2 / (3k_B(T - \theta_p))$, where μ_{eff} is the effective magnetic moment, θ_p is the Weiss temperature, N_A is the Avogadro number and k_B is the Boltzmann constant. From the least-square fits shown as white lines in Fig. 2 (a) and (b), values of $\mu_{\text{eff}} = 3.30 \mu_B/\text{Pr}$, $\theta_p = 95.10$ K and $\mu_{\text{eff}} = 3.15 \mu_B/\text{Pr}$, $\theta_p = 99.16$ K for PrPt₄Ag and PrPt₄Au, respectively are obtained. These values of μ_{eff} are slightly reduced in comparison to the value of $3.58 \mu_B/\text{Pr}$ calculated for a free Pr³⁺ ion. Such reduction in μ_{eff} can be attributed to the crystalline electric field (CEF) effect on the Pr³⁺ moment. The isothermal magnetization for both compounds measured at temperatures of 1.8 K and 10 K are shown in the insets to Fig. 2 (a) and (b). The magnetization trend shows a little curvature at 10 K which becomes more pronounced at 1.8 K for both compounds. PrPt₄Ag and PrPt₄Au attain magnetization of $\approx 1.8 \mu_B/\text{Pr}$ at 7 T, which is about 50% reduced compared to the value of $3.2 \mu_B/\text{Pr}$ expected for a free Pr³⁺ ion. Assuming that at a temperature of 1.8 K no higher-lying levels of the $J = 4$ multiplet of Pr are occupied, we attribute this deficiency in the extracted magnetization to the effects of magneto-crystalline anisotropy in both compounds.

4. Specific heat

The temperature dependence of the specific heat $C_p(T)$ between 1.9 K and 300 K for PrPt₄Ag and PrPt₄Au are shown in Fig. 3 (a) and (b). Values of ≈ 150 J/(mol K) are observed at room temperature for both compounds, which correspond to the Dulong-Petit value. In inset (i) of Fig. 3 (a), the low- T plot of C_p/T against T for PrPt₄Ag is shown. At 7.6 K an anomaly with a broad feature is observed. The electrical resistivity results to be presented in Section 5 also

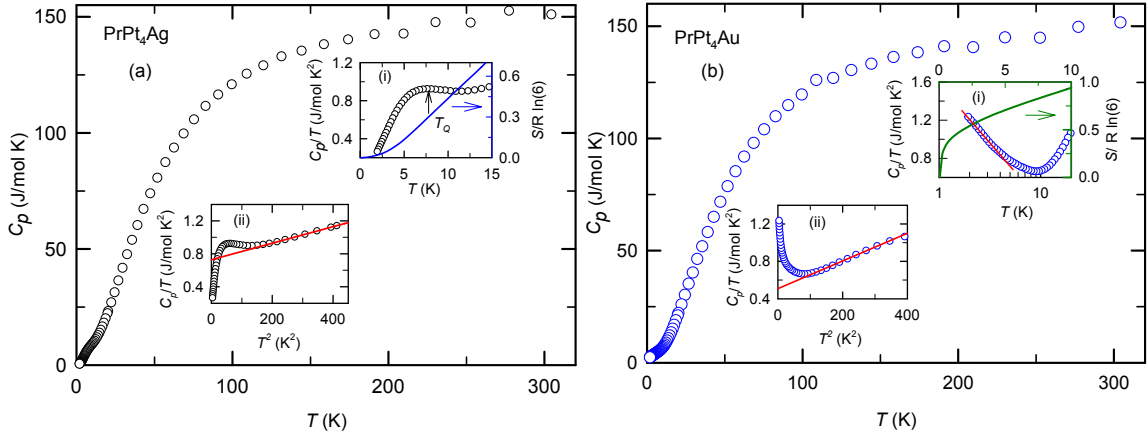


Figure 3. (a) Temperature dependence of specific heat $C_p(T)$ of PrPt_4Ag . Inset (i): Low- T plot of C_p/T against T with the arrow indicating the phase transition at T_Q . Also shown is the calculated entropy (blue line) with axis on the right. Inset (ii): Plot of C_p/T against T^2 for PrPt_4Ag together with a linear fit (red line) to extract the Sommerfeld coefficient. (b) Plot of C_p against T for PrPt_4Au . Inset (i): Plot of C_p/T against T on a semi-log axis. The red line is a guide to the eye indicating a logarithmic divergence of $C_p(T)/T$. The calculated entropy (green line) is also shown with axis on the right. Inset (ii): Plot of C_p/T against T^2 for PrPt_4Au together with a linear fit (red line) to extract the Sommerfeld coefficient.

reveal an anomaly around the same temperature. No such an anomaly is however observed in $\chi(T)$ presented in the previous section, thus suggesting a possible multipolar ordering of the Pr^{3+} moment in PrPt_4Ag . This is supported by the Van-Vleck paramagnetism observed in $\chi(T)$ indicating that spins or dipolar order do not play a detectable role in the anomaly. In the absence of a long-range magnetic order in Pr systems, the $4f$ -electrons orbitals are the only effective degrees of freedom and multipolar ordering of the Pr^{3+} moment can be realized [10, 11]. Also shown is the plot of the calculated entropy. At T_Q only an amount of $0.3R\ln(6)$ is released which is only about one third of the total entropy expected. The plot of C_p/T against T on a semi-log scale for PrPt_4Au shown in inset (i) of Fig. 3 (b) shows an upturn below 10 K reaching a value of $1.23 \text{ J}/(\text{mol K}^2)$ at 1.9 K. We have also observed a linear-in- T behavior of $\rho(T)$ which is discussed in Section 5. These observations in PrPt_4Au are the hallmark of a non-Fermi liquid (nFL) behavior. Among many other reasons, proximity to a quantum critical point or possible spin/elemental disorder such as in doped systems could be responsible for such behavior [12]. The calculated entropy is also presented in the same plot. At 8 K, the recovered entropy is about $0.9R\ln(6)$ which is close to the full entropy expected.

We further analyzed the low- T behavior by plotting of C_p/T against T^2 for both compounds as shown in inset (ii) of Fig. 3 (a) and inset (ii) of Fig. 3 (b). Least-square fits to both sets of data (represented as red lines) based on the expressions: $C_p/T = \gamma + \beta T^2$ and $\beta = 12\pi^4 nR/(5\theta_D^3)$, where n and R are the number of atoms per formula unit and universal gas constant, respectively, γ is the Sommerfeld coefficient and θ_D is the Debye temperature are shown. From the fits, $\gamma = 728.50 \text{ J}/(\text{mol K}^2)$ and $509.10 \text{ J}/(\text{mol K}^2)$ are obtained for PrPt_4Ag and PrPt_4Au , respectively. The observed γ values for these two compounds are more than two orders of magnitude greater than what is expected for an ordinary metal and qualitatively similar to those of the heavy fermion (HF) systems, where significant enhancement of the quasiparticles mass have been observed [13].

Table 2. A collection of estimated characteristic HF parameters of PrPt₄Ag and PrPt₄Au.

Compound	γ (mJ/(mol _{Pr} K ²))	A ($\mu\Omega\text{cm}/\text{K}^2$)	A/γ^2 ($\times 10^{-5}\mu\Omega\text{cm}(\text{mol}_{\text{Pr}}\text{K}/\text{mJ})^2$)	R_w
PrPt ₄ Ag	728.50	0.010	0.00188	1.38
PrPt ₄ Au	509.10	0.117	0.0449	1.62

5. Electrical transport

The temperature dependence of the electrical resistivity $\rho(T)$ for PrPt₄Ag and PrPt₄Au investigated between 1.9 K and 300 K are presented in Fig. 4 (a) and (b), respectively. The observed values of residual resistivity are ≈ 6 and ≈ 3 for PrPt₄Ag and PrPt₄Au, respectively. Both compounds show typical metallic behavior down to low temperatures. A broad curvature is observed at intermediate temperatures in PrPt₄Ag, which is common to rare-earth intermetallic systems; possibly associated to thermal de-population of the crystal field levels as temperature is lowered. A plot of $\rho(T)$ against T^2 presented in the inset of Fig. 4 (a) indicates a power law behavior based on the expression: $\rho(T) = \rho_0 + AT^2$. A fit of the expression to the data is shown as the red line. The residual resistivity, $\rho_0 = 10.46 \mu\Omega\text{cm}$ and the coefficient of the quadratic term, $A = 0.010 \mu\Omega\text{cm}/\text{K}^2$ are obtained. The Kadowaki-Woods ratio (KWR) [14], $A/\gamma^2 = 1.88 \times 10^{-8} \mu\Omega\text{cm}(\text{mol K}/\text{mJ})^2$ is obtained by using $\gamma = 728.5 \text{ mJ}/(\text{mol K}^2)$ obtained from $C_p(T)$ analysis. The relationship between $\chi(T)$ and γ is also evaluated using the Wilson ratio [15] given as: $R_w = \pi^2 k_B^2 \chi(T \rightarrow 0)/(\mu_{\text{eff}}^2 \gamma)$. Using the observed low- T values of $\chi(T \rightarrow 0) = 0.5025 \text{ emu/mol}$, $\gamma = 728.5 \text{ mJ}/(\text{mol K}^2)$ and $\mu_{\text{eff}} = 3.30 \mu_B/\text{Pr}$ yields $R_w = 1.38$ which is comparable to a value of unity expected for HF systems. Also, a little anomaly is noticeable in the low- T plot at ~ 7.6 K which coincides with the anomaly observed in $C_p(T)$ around the same temperature.

PrPt₄Au on the other hand is quasi-linear in nature down to low temperatures. In the inset of Fig. 4 (b), the low- T behavior of PrPt₄Ag is shown together with a fit (shown as red line) using the expression; $\rho(T) = \rho_0 + AT^n$. From the fit, the residual resistivity, $\rho_0 = 14.58 \mu\Omega\text{cm}$, $n = 1$ and $A = 0.117 \mu\Omega\text{cm}/\text{K}$ are obtained. Such a temperature dependence of $\rho(T)$ deviates from the Fermi-liquid behavior expected at low temperatures for normal metals. Results from $C_p(T)$ of PrPt₄Au discussed in Section 4 have also shown a temperature dependence that deviates from those of ordinary metals. Using the values of $A = 0.117 \mu\Omega\text{cm}/\text{K}^2$ and $509.10 \text{ mJ}/(\text{mol K}^2)$, yields $\text{KWR} = 4.49 \times 10^{-7} \mu\Omega\text{cm}(\text{mol K}/\text{mJ})^2$. Also, using the values of $\chi(T \rightarrow 0) = 0.3743 \text{ emu/mol}$, $\gamma = 509.10 \text{ mJ}/(\text{mol K}^2)$ and $\mu_{\text{eff}} = 3.15 \mu_B/\text{Pr}$ yields $R_w = 1.62$. The parameters observed in PrPt₄Ag and PrPt₄Au reveal both compounds as new HF systems.

6. Discussion and conclusion

The existence of the hexagonal PrPt₄Ag and PrPt₄Au compounds are reported together with their physical and magnetic properties. PrPt₄Ag shows a putative multipolar ordering at $T_Q = 7.6$ K. From the crystal field levels permitted for the $J = 4$ multiplet in a D_{6h} local symmetry, one would expect to have 3 Γ_3 non-Kramers doublets and another 3 Γ_1 singlets. However, the observation of such an anomaly at T_Q makes Γ_3 the likely ground state in PrPt₄Ag. In contrast, the low- T region of PrPt₄Au shows a logarithmic divergence of $C_p(T)/T$, and a linear-in- T behavior of $\rho(T)$ below 10 K which is typical of a non-Fermi liquid behavior. These behaviors are likely associated with spin scatterings observed for a system in the proximity of a quantum critical point. Further analyses of $C_p(T)$ of both compounds reveal $\gamma = 728.50 \text{ J}/(\text{mol K}^2)$ and $509.10 \text{ J}/(\text{mol K}^2)$ for PrPt₄Ag and PrPt₄Au, respectively. In Table 2, a collection of characteristic HF parameters are presented for easy comparison with the observations in this work. The observation of enhanced γ value in systems with a Γ_3 non-Kramers ground state are often associated to the quadrupolar Kondo effect [10, 11]. Future studies will focus on

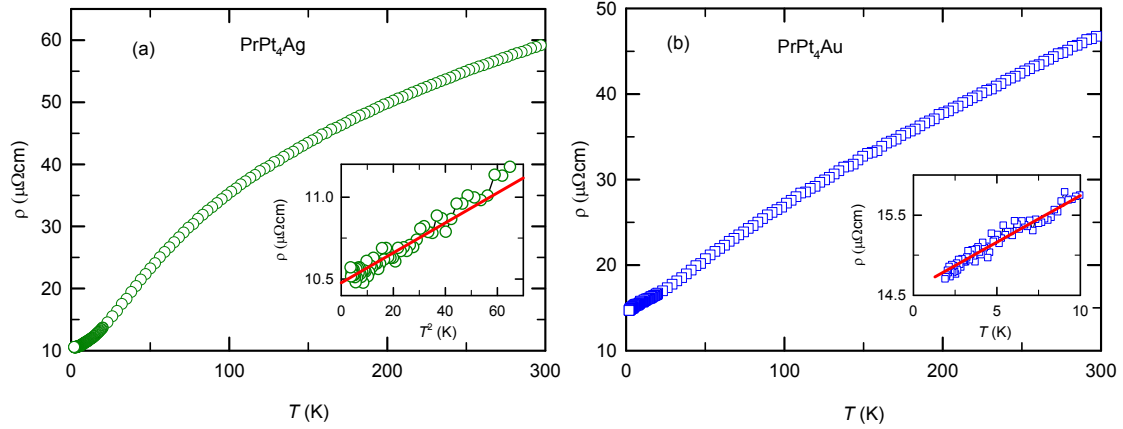


Figure 4. (a) Temperature dependence of electrical resistivity, $\rho(T)$, of PrPt_4Ag . Inset: Low- T plot of ρ against T^2 together with a fit (red line) described in the text. (b) Plot of $\rho(T)$ against T of PrPt_4Au . Inset: Low- T plot of ρ and the red line is a fit described in the text.

experiments below 2 K in order to further unravel the physics involved in the ground state of these two non-Kramers-ion systems.

Acknowledgment

MOO acknowledges the UJ-URC bursary for doctoral studies in the Faculty of Science. AMS thanks the SA-NRF (93549) and UJ-URC for financial support.

References

- [1] Andres K and Bucher E 1970 *Phys. Rev. Lett.* **24** 1181
- [2] Buschow K H J 1972 *J. Less Common Met.* **29** 283
- [3] Narasimhan K S V L, Rao V U S and Butera R A 1973 *AIP Conf. Proc.* **10** 1081
- [4] Karaki Y, Yotsui K, Kubota M and Ishimoto H 2000 *Physica B* **284-288** 1688
- [5] Malik S K, Vijayaraghavan R, Adroja D T, Padalia B D and Edelstein A S 1990 *J. Magn. Mater.* **92** 80
- [6] Zhang S, Mizushima T, Kuwai T and Isikawa Y 2009 *J. Phys. Condens. Matter* **21** 205601
- [7] Zhang S, Isikawa Y, Tayama T, Kuwai T, Mizushima T, Akatsu M, Nemoto Y and Goto T 2010 *J. Phys. Soc. Jpn.* **79** 114707
- [8] Thompson P, Cox D E and Hastings J B 1987 *J. Appl. Crystallogr.* **20** 79
- [9] Rodríguez-Carvajal J 1993 *Physica B* **192** 55
- [10] Suzuki O, S Suzuki H, Kitazawa H, Kido G, Ueno T, Yamaguchi T, Nemoto Y and Goto T 2005 *J. Phys. Soc. Jpn.* **75** 013704
- [11] Tanida H, S Suzuki H, Takagi S, Onodera H and Tanigaki K 2006 *J. Phys. Soc. Jpn.* **75** 073705
- [12] Schofield A J 1999 *Contemp. Phys.* **40** 95
- [13] Ogunbunmi M O, Sondezi B M, Nair H S and Strydom A M 2018 *Physica B* **536** 128
- [14] Kadowaki K and Woods S B 1986 *Solid State Commun.* **58** 507
- [15] Wilson K G 1975 *Rev. Mod. Phys.* **47** 773